journal

J. Am. Ceram. Soc., 90 [7] 2220–2225 (2007)
DOI: 10.1111/j.1551-2916.2007.01708.x

Reaction Between Titanium and Zirconia Powders During Sintering at 1500°C

Kun-Lin Lin and Chien-Cheng Lin*,†

Department of Materials Science and Engineering, National Chiao Tung University, Hsinchu 30050, Taiwan

Zirconia–titanium (ZrO_2–Ti) composites have been considered potential thermal barrier graded materials for applications in the aerospace industry. Powder mixtures of Ti and 3 mol% Y_2O_3 partially stabilized ZrO_2 in various ratios were sintered at 1500°C for 1 h in argon. The microstructures of the as-sintered composites were characterized by X-ray diffraction and transmission electron microscopy/energy-dispersive spectroscopy. Ti reacted with and was mutually soluble in ZrO_2, resulting in the formation of α-Ti(O, Zr), Ti_2ZrO, and/or TiO. These oxygen-containing phases extracted oxygen ions from ZrO_2, whereby oxygen-deficient ZrO_2 was generated. For relatively small Ti/ZrO_2 ratios, specimens with ≤30 mol% Ti, TiO were formed as oxygen could be sufficiently supplied by excess ZrO_2. For the specimens with ≥50 mol% Ti, lamellar Ti_2ZrO was precipitated in α-Ti(Zr, O), with no TiO being found. Both *m*-ZrO_{2-x} and *t*-ZrO_{2-x} were found in specimens with ≤50 mol% Ti; however, only *c*-ZrO_{2-x} was formed in the specimen with 70 mol% Ti. As ZrO_2 was gradually dissolved into Ti, yttria was retained in ZrO_2 because of the very limited solubility of yttria in α-Ti(O, Zr) or TiO. The concentration of retained yttria and the degree of oxygen deficiency in ZrO_2 increased with the Ti content. The complete dissolution of ZrO_2 into Ti was followed by the precipitation of $Y_2Ti_2O_7$ in the specimen with 90 mol% Ti.

I. Introduction

It is well known that partially stabilized zirconia (PSZ) has good toughness for wide structural applications,[1,2] and its mechanical properties can be enhanced by incorporating titanium (Ti).[3–8] Weber *et al.*[3] found that sintered zirconia (ZrO_2) crucibles containing 15 at.% Ti showed good strength and thermal shock resistance. Arias[6,7] investigated the thermal shock resistance of ZrO_2 with 15 mol% Ti after sintering at 1870°C for 1 h in vacuum, claiming that the grain growth of ZrO_2 was inhibited due to the addition of Ti so that both thermal shock resistance and strength were increased. For ZrO_2 with 5–15 mol% Ti sintered at 1740°C for 1 h under a vacuum of 10^{-1}–10^{-2} torr, Lin *et al.*[8] reported that the ZrO_2 was partially stabilized as cubic and tetragonal phases, and its thermal shock resistance was significantly improved because of the dissolution of TiO. However, without taking into account possible reactions between Ti and ZrO_2, they hypothesized that the formation of TiO was caused by residual oxygen in the vacuum furnace.

In the past decade, ZrO_2–Ti functionally graded materials (FGMs) have been considered potential thermal barrier graded materials for applications in the aerospace industry. For the ZrO_2–Ti FGMs, Teng and colleagues[9,10] showed that only α-Ti(O), tetragonal (*t*)-ZrO_2, and *m*-ZrO_2 were found in various Ti/ZrO_2 composites after annealing from 1400° to 1650°C. They reported that the volume fraction of *m*-ZrO_2 increased with the Ti content in the Ti/ZrO_2 composites, while the interfacial stresses, arising from the plastic deformation of Ti and the thermal expansion mismatch of Ti and ZrO_2, were the driving forces for the phase transformation from *t*-ZrO_2 to *m*-ZrO_2.

The interfacial reaction between Ti and ZrO_2 has been studied in the past few decades.[3–5,11–13] These studies indicated that oxygen was dissolved into Ti, causing the ZrO_2 to become oxygen-deficient and blackened. Distinct reaction layers were formed at the interface between Ti and ZrO_2.[5,14–17] Lin and Lin[14,16–21] have conducted an investigation on the diffusional reaction between Ti and ZrO_2 at temperatures ranging from 1100° to 1550°C using transmission electron microscopy/energy-dispersive spectroscopy (TEM/EDS), electron probe microanalysis (EPMA), and scanning electron microscopy (SEM)/EDS. They found that α-Ti, β′-Ti, the ordered Ti suboxide (Ti_3O), and lamellar and spherical Ti_2ZrO were formed after annealing from 1100° to 1700°C.[14,20] At the ZrO_2 side far away from the interface of Ti/ZrO_2, Lin and Lin[21] observed twinned *t*′-ZrO_{2-x}, lenticular *t*-ZrO_{2-x}, ordered *c*-ZrO_{2-x}, and intergranular α-Zr after reaction at 1550°C.

The review of the literature implies that some contradictions exist with respect to the reaction products and the origin of oxygen in Ti oxides and/or solid solutions. In the present study, powder mixtures of Ti and ZrO_2 in various ratios were sintered at 1500°C for 1 h in argon. The microstructures of the as-sintered composites were characterized using X-ray diffraction (XRD) and TEM/EDS. The reaction mechanisms between Ti and ZrO_2 were elucidated.

II. Experimental Procedure

The starting powders used in this study were 3 mol%Y_2O_3 PSZ (>94 wt% ZrO_2+HfO_2, 5.4 wt% Y_2O_3, <0.001 wt% Fe_2O_3, <0.01 wt% SiO_2, <0.005 wt% Na_2O, <0.005 wt% TiO_2, < 0.02 wt% Cl, <0.005 wt% SO_4^{2-}, 0.3 μm in average, Toyo Soda Mfg. Co., Tokyo, Japan), and commercially pure Ti (with a nominal composition of 99.31 wt% Ti, 0.25 wt% O, 0.01 wt% H, 0.03 wt% N, 0.10 wt% C, 0.30 wt% Fe., 60–70 μm average diameter, Alfa Aesar, Ward Hill, MA). Several composites in various Ti/ZrO_2 ratios were prepared by pressureless sintering. The compositions and designations are summarized in Table I. The Ti/ZrO_2 composites contained 10, 30, 50, 70, and 90 mol% Ti, respectively, with ZrO_2 in residue. The composite containing 10 mol% Ti and 90 mol% ZrO_2 was designated as 10T90Z, and so on.

The mixtures of ZrO_2 and Ti powders were ball milled (with ZrO_2 milling media) in ethanol (containing 1 wt% polyvinyl alcohol, or PVA, as a binder for forming green bodies) for 24 h. The slurries were dried in an oven at 150°C, ground with an agate mortar and pestle, and then shaken vigorously in a plastic bottle. The powder mixtures were pressed into disks (10 mm in diameter × 3 mm thick) at a pressure of 150 MPa and then sintered in argon at 1500°C for 1 h at 10° and 5°C/min heating and cooling rates, respectively.

T. Besmann—contributing editor

Manuscript No. 22492. Received November 14, 2006; approved February 15, 2007.
Research supported by National Science Council of Taiwan under Contract No. NSC 94-2216-E-009-011.
*Member, American Ceramic Society.
†Author to whom correspondence should be addressed. e-mail: chienlin@faculty.nctu.edu.tw

Table I. Compositions of Ti/ZrO_2 Composites

Specimens[†]	Composition (mol%)
90T10Z	90 mol % Ti+10 mol% ZrO_2
70T30Z	70 mol % Ti+30 mol% ZrO_2
50T50Z	50 mol % Ti+50 mol% ZrO_2
30T70Z	30 mol % Ti+70 mol% ZrO_2
10T90Z	10 mol % Ti+90 mol% ZrO_2

[†]The powder mixtures were pressed into disks at a pressure of 150 MPa and then sintered at 1500°C/1 h in argon.

After sintering, the linear shrinkage (a) was calculated by the following equation: $a = [(d_0-d)/d_0] \times 100\%$, where d_0 and d are the measured diameters of the green body and the sintered Ti/ZrO_2 composite, respectively. The apparent densities (ρ_a) of all the Ti/ZrO_2 powder mixtures were measured by gas pycnometry using 99.99% pure helium gas (Model MultiVolume Pycnometer 1305, Micromeritics, Norcross, GA). The bulk densities (ρ_b) of the sintered Ti/ZrO_2 composites were determined by the Archimedes method using water as an immersed medium. For a nonporous powder, its apparent density approximates to the true density and can be used as the reference point in calculating the percentage of the theoretic density of a sintered body. Thus, the relative densities (ρ_{rb}) of the sintered specimens were given as follows: $\rho_{rb} = (\rho_b/\rho_a) \times 100\%$, assuming that the change in density owing to the reaction was negligible. This assumption is reasonable as most of the reaction products are ZrO_{2-x} and α-Ti(O, ZrO_2)- derived compounds (e.g. α-Ti(O, Zr), Ti_2ZrO, and TiO). The only concern is $Y_2Ti_2O_7$; however, its amount is insignificant with respect to other phases. Then, the relative densities (ρ_{rg}) of the green bodies were calculated by the following relationship: $\rho_{rg} = \rho_{rb} \times (1-a)^3$.

The microstructural characterization of sintered Ti/ZrO_2 composites was carried out using an x-ray diffractometer (Model MXP18, Mac Science, Yokohama, Japan) and an analytical transmission electron microscope (Model Tecnai 20, Philips, Eindhoven, the Netherlands) equipped with an energy-dispersive x-ray spectrometer (Model ISIS 300, Oxford Instruments Inc., London, U.K). The measurement conditions of XRD were Cu$K\alpha$ radiation at 50 kV, 150 mA, and a scanning rate of 2°/min. The TEM specimens were cut, ground, polished, dimpled, and then ion milled by standard procedures. The Cliff–Lorimer[22] standardless technique was used to analyze the compositions of the various phases. However, the compositions of oxygen-deficient ZrO_2 in various Ti/ZrO_2 composites were measured using stoichiometric ZrO_2 as a standard.

III. Results and Discussion

(1) Appearance, Shrinkage, and Densities of Sintered Bodies

Figures 1(a) and (b) display the photographs of the green bodies and the sintered Ti/ZrO_2 composites, respectively. For green bodies, the 90T10Z appeared dark gray, while the 10T90Z was light gray. After sintering, the 90T10Z had a metallic luster similar to Ti. However, the sintered 10T90Z became blackened as it was mainly composed of oxygen-deficient ZrO_2 after sintering at 1500°C/1 h in argon. Obviously, the color of the sintered 10T90Z was similar to that of oxygen-deficient ZrO_2.

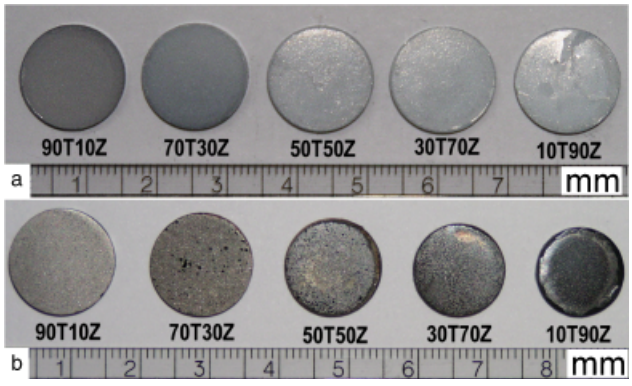

Fig. 1. (a) Ti/ZrO_2 green bodies; (b) sintered composites after sintering at 1500°C/1 h in argon.

Table II. Linear Shrinkages (a), Apparent Densities of Powder Mixtures (ρ_a), Calculated Relative Densities of Green Bodies (ρ_{rg}), and Bulk Densities (ρ_b) and Relative Densities (ρ_{rb}) of Sintered Bodies

Specimen	A[†] (%)	ρ_a (g/cm^3)	ρ_{rg}[‡](%)	ρ_b (g/cm^3)	ρ_{rb} (%)
90T10Z	0.8	4.07	83	3.48	85
70T30Z	2.6	4.27	80	3.69	86
50T50Z	8.4	4.57	68	4.05	88
30T70Z	13.1	4.64	60	4.26	92
10T90Z	16.2	5.02	58	4.94	98

[†]Calculated by $a = [(d_0-d)/d_0] \times 100\%$, where d_0 and d are the measured diameters of the green and the sintered bodies, respectively. [‡]Calculated by $\rho_{rg} = \rho_{rb} \times (1-a)^3$.

The linear shrinkage (a) of the sintered Ti/ZrO_2 composites with respect to their corresponding green bodies is shown in Table II. It was found that the linear shrinkage of the sintered Ti/ZrO_2 composite increased with increasing ZrO_2 content. Table II also shows the measured apparent densities (ρ_a) of powder mixtures and the measured bulk densities (ρ_b) of sintered Ti/ZrO_2 composites. The relative density (ρ_{rb}) of the sintered body, calculated by $\rho_{rb} = \rho_b/\rho_a \times 100\%$, increased with increasing ZrO_2 content due to a decrease in the porosity. It was noticeable that the sintered 10T90Z had a high relative density of about 98%. The densification of Ti/ZrO_2 composites by solid-state sintering could have been enhanced by the highly active major component, i.e., submicrometer ZrO_2. In contrast, the relative density of the green body increased with increasing Ti content as Ti particles underwent plastic deformation during cold pressing. The calculated relative density (ρ_{rg}) of the 90T10Z green body was about 83%, while that of the 10T90Z green body was about 58%. However, the densification of the 90T10Z was insignificant (about 2%) during sintering probably due to the very large particle size of Ti powder, which was 60–70 μm in diameter.

(2) XRD Analyses

Figure 2 shows the XRD spectra of various sintered Ti/ZrO_2 composites. The sintered 10T90Z consisted of m-ZrO_2, t-ZrO_2, and TiO; however, no peaks of α-Ti were observed. The α-Ti appeared in all specimens except in the sintered 10T90Z. Ti_2ZrO instead of TiO was found in sintered composites containing more than 50 mol% Ti.

As for ZrO_2, cubic (c)-ZrO_2 and t-ZrO_2 could be distinguished by the splitting {002} and {200} reflections of the t-ZrO_2. By comparing the XRD spectra of the sintered 10T90Z, 30T70Z, and 50T50Z, it was seen that the (002) reflection peak of t-ZrO_2 was gradually diminished with decreasing ZrO_2 content. The (002) and (200) reflections of t-ZrO_2 were eventually replaced by the (200) reflection of c-ZrO_2 in the sintered 70T30Z. c-ZrO_2 was fully stabilized in the sintered 70T30Z as excessive Ti gave rise to a large concentration of oxygen vacancies in ZrO_2.[22] The stabilization of c-ZrO_2 was unlikely to be caused by the grain size, because the ZrO_2 grain grew appreciably up to about 2.5–4 μm in the sintered 70T30Z [see Fig. 5(a)]. Neither m-ZrO_2 nor t-ZrO_2 peaks were found in the sintered 70T30Z and 90T10Z. Furthermore, a trace of c-ZrO_2 remained in the sintered 90T10Z because ZrO_2 was almost dissolved in Ti.

The present results were inconsistent with those reported by Teng *et al.*,[9,10] who found only t-ZrO_2 and m-ZrO_2, but no c-ZrO_2, Ti_2ZrO, or $Y_2Ti_2O_7$ (shown in the TEM analyses), in various Ti/ZrO_2 composites. They also indicated that the

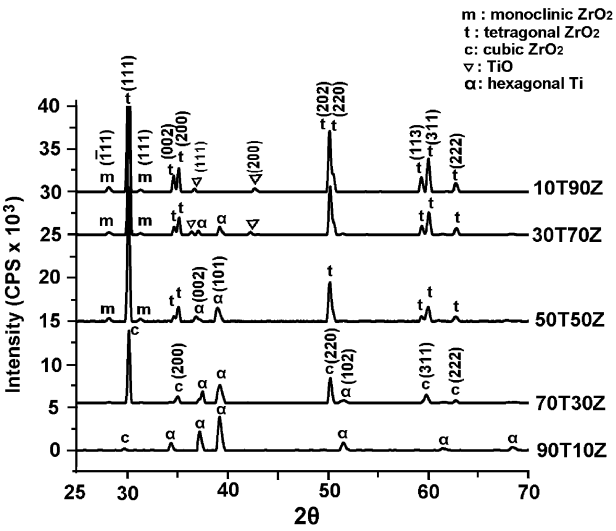

Fig. 2. X-ray diffraction spectra of Ti/ZrO_2 composites.

volume fraction of *m*-ZrO_2 in Ti/ZrO_2 composites increased with the Ti content, and the interfacial stress arising from the thermal expansion mismatch and the plastic deformation of Ti enhanced the *t*-$ZrO_2 \rightarrow$ *m*-ZrO_2 transformation.[10] However, in the present study, the amount of *m*-ZrO_2 decreased with increasing Ti content, as the reaction between Ti and ZrO_2 gave rise to retained yttria and oxygen vacancies, of which the concentrations in ZrO_2 increased with the Ti content. It was also noted that the *c*-ZrO_2 was fully stabilized due to the high concentrations of retained yttria and oxygen vacancies in ZrO_2 of the sintered 70T30Z.

(3) Microstructures of Various Ti/ZrO_2 Composites

Figure 3(a) shows a bright-field image of TiO, *m*-ZrO_{2-x}, and (*t*+*m*)-ZrO_{2-x} in the 10T90Z after sintering at 1500°C/1 h. Based on the Ti distribution, it appeared that hard ZrO_2 particles were embedded in soft Ti particles, which were subjected to plastic deformation during cold pressing. Figures 3(b) and (c) show the selected area diffraction patterns (SADPs) of TiO with [001] and [111] zone axes, respectively. TiO has the B1(NaCl) structure and its lattice parameter was calculated as 4.43 Å. From the EDS spectrum, shown in Fig. 3(d), TiO dissolved a significant amount of ZrO_2 and was composed of 45.7 at.% Ti, 50.2 at.% O, and 4.2 at.% Zr. It indicated that the stabilizer of ZrO_2 (i.e. yttria) was not dissolved into TiO within the limits of detection of EDS. Figure 3(e) shows the EDS spectrum of *m*-ZrO_{2-x}, which consisted of 57.6 at.% Zr, 40.5 at.% O, and 1.8 at.% Y, corresponding to $ZrO_{1.39}$ with Y_2O_3 in solid solution. Figure 3(f) shows the SADPs, as well as the redrawn diagram, of (*t*+*m*)-ZrO_{2-x} with $[011]_t//[011]_m$ and $(200)_t//(100)_m$. The small lathe of *m*-ZrO_{2-x} originated at the grain boundaries of *t*-ZrO_{2-x} with a stress-field contrast (labeled as "*t*+*m*" in Fig. 3(a)), owing to the stress concentrations at such a region.[23,24] For the sintered 10T90Z and 30T70Z, the interfacial stress field arose from the thermal expansion mismatch and plastic deformation of Ti or TiO, resulting in an enhanced driving force for the *t*-$ZrO_{2-x} \rightarrow$ *m*-ZrO_{2-x} transformation.[10] Several martensite lathes have grown completely across the grain and changed to twinned *m*-ZrO_{2-x} (labeled as "m" in Fig. 3(a)). Figure 3(g) shows the SADP, as well as the redrawn diagram, of *m*-ZrO_{2-x} with the [111] zone axis. The twinning plane of *m*-ZrO_{2-x} was identified to be $(0\,\bar{1}\,1)$. It was noted that part of Ti was also oxidized and became TiO in the sintered 30T70Z as well.

Figure 4(a) displays the bright-field image of α-Ti(Zr, O), *m*-ZrO_{2-x}, and (*t*+*m*)-ZrO_{2-x} in the 50T50Z composite after sintering at 1500°C/1 h. For comparison, the oxide TiO was found in the sintered 10T90Z instead of α-Ti(Zr, O). As the Ti content increased above 50 mol%, α-Ti(Zr, O) rather than TiO was formed because the supply of oxygen from ZrO_2 was limited compared with the ZrO_2-rich composites. Based upon the Ti–O phase diagram[25] and EDS results (Table III), α-Ti dissolved <33 at.% O and the O/Zr ratio was <1.14 in composites containing $\geq$ 50 mol% Ti. As shown in Fig. 4(a), the α-Ti(Zr, O) contained many dislocations, which were likely caused by the

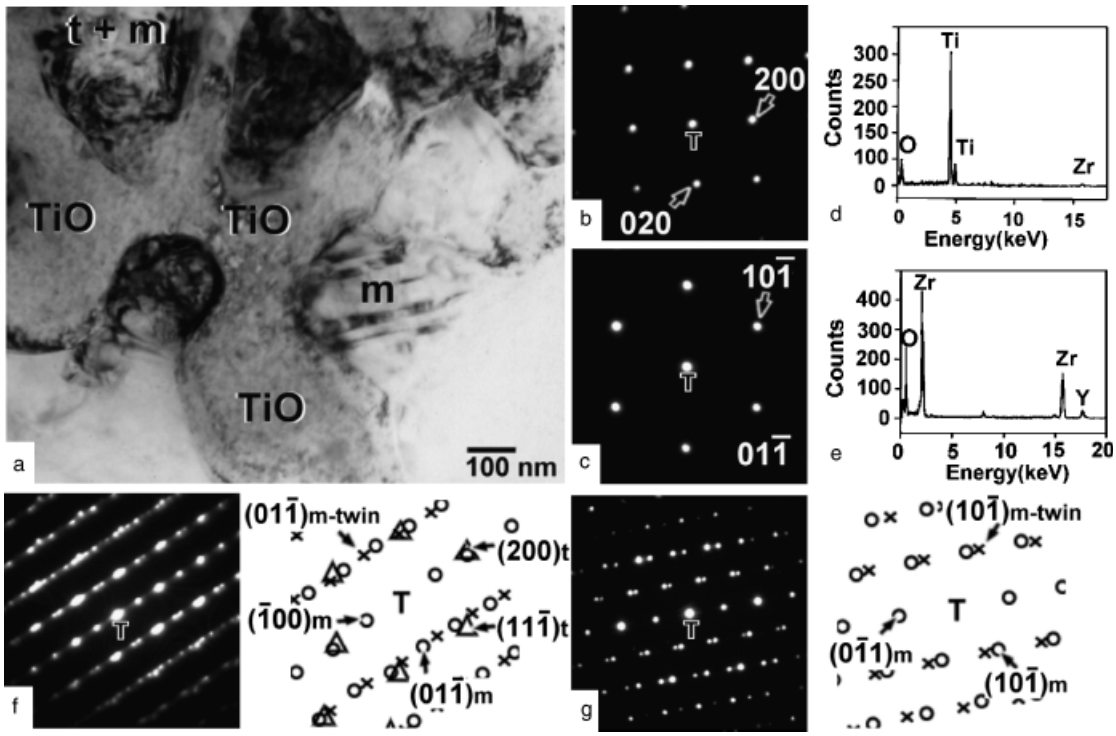

Fig. 3. (a) Transmission electron micrograph (bright-field image) of TiO, *m*-ZrO_{2-x}, and (*t*+*m*)-ZrO_{2-x} in the 10T90Z composites after sintering at 1500°C/1 h; (b) and (c) selected area diffraction patterns (SADPs) of TiO with the [001] and [111] zone axes, respectively; (d) and (e) energy-dispersive spectra of TiO and *m*-ZrO_{2-x}, respectively; (f) SADPs of the (*t*+*m*)-ZrO_{2-x} along the $[011]_t$ or $[011]_m$ zone axis; (g) an SADP of the *m*-ZrO_{2-x} along the [111] zone axis. Note that the SADPs in (f) and (g) were redrawn, respectively (Δ, *t* -ZrO_{2-x}; ○, *m*-ZrO_{2-x}; ×, *m*-ZrO_{2-x} twin).

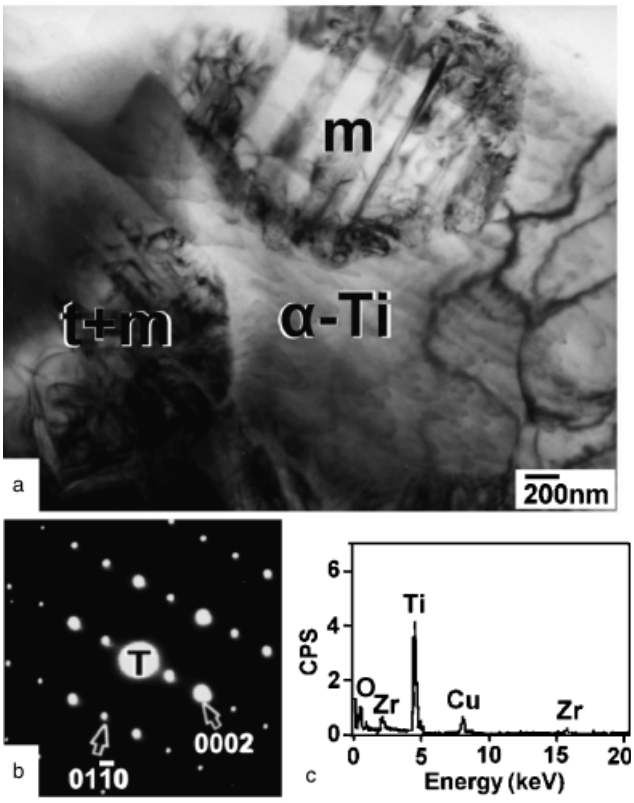

Fig. 4. (a) Transmission electron micrograph (bright-field image) of α-Ti, *m*-ZrO_{2-x}, and (*t*+*m*)-ZrO_{2-x} in the 50T50Z composite after sintering at 1500°C/1 h; (b) a selected area diffraction pattern of α-Ti(Zr, O) along the [2 $\bar{1}$ $\bar{1}$ 0] zone axis; and (c) an energy-dispersive spectrum of α-Ti(Zr, O).

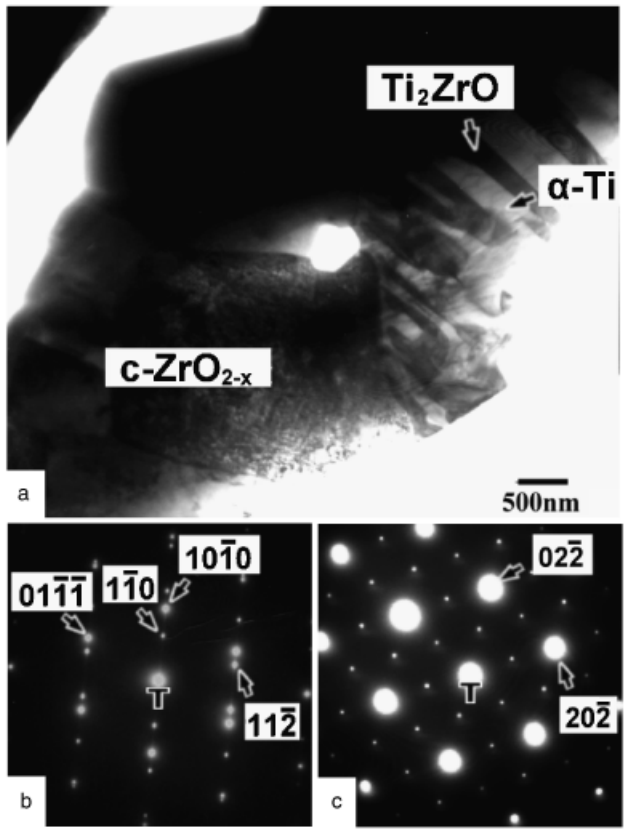

Fig. 5. (a) Transmission electron micrograph (bright-field image) of *c*-ZrO_{2-x} and lamellae α-Ti+Ti_2ZrO in the 70T30Z composite after sintering at 1500°C/1 h; (b) selected area diffraction patterns (SADPs) of α-Ti and Ti_2ZrO along the zone axes of $[111]_{Ti2ZrO}$// $\bar{1}$ 2 $\bar{1}$ $3_{\alpha\text{-Ti}}$; (c) an SADP of *c*-ZrO_{2-x} along the zone axis of [111].

extended plastic deformation during fabrication. Dislocations disappeared when Ti was oxidized as TiO as illustrated in Fig. 3(a). Figure 4(b) displays the SADP of α-Ti(Zr, O) with the [2 $\bar{1}$ $\bar{1}$ 0] zone axis. The lattice constants of hexagonal α-Ti(Zr, O) were calculated to be $a \approx 3.27$ Å and $c \approx 4.92$ Å. Significant amounts of Zr and O were dissolved into the α-Ti. Figure 4(c) shows the EDS spectrum of α-Ti(Zr, O), revealing that it comprised 73.5 at.% Ti, 7.9 at.% Zr, and 18.6 at.% O. The solubility limit of ZrO_2 in Ti was reported to be up to approximately 10 mol% in an early study conducted by Ruh.[4] Figure 4(c) also shows that the solubility of yttria was very limited in α-Ti(O, Zr).

In previous studies,[8–10] Ti/ZrO_2 composites with more than 50 mol% Ti showed no Ti-containing phases except for α-Ti (Zr, O). However, Ti_2ZrO was precipitated in α-Ti(Zr, O) when the Ti content increased above 50 mol% in the present study. Figure 5(a) shows the bright-field image of *c*-ZrO_{2-x} and the lamellae of α-Ti+Ti_2ZrO in the sintered 70T30Z. From the SADPs shown in Fig. 5(b), the lamellar phases (α-Ti+Ti_2ZrO) were identified as orthorhombic Ti_2ZrO and hexagonal α-Ti, respectively, with the orientation relationship of $[111]_{Ti_2ZrO}//[\bar{1}2\bar{1}3]_{\alpha-Ti}$ and $(1\bar{1}0)_{Ti_2ZrO}//(10\bar{1}0)_{\alpha\text{-Ti}}$. The lattice constants of the Ti_2ZrO orthorhombic unit cell were calculated to be $a_o \approx 4.91$ Å, $b_o \approx 8.21$ Å, and $c_o \approx 3.19$ Å, and those of the α-Ti hexagonal unit cell were $a_h \approx 3.11$ Å, $c_h \approx 4.72$ Å. The lamellae of α-Ti+Ti_2ZrO had been found in the Ti/ZrO_2 diffusion couple[16,20]; however, they were not found previously in Ti/ZrO_2 composite systems. The *c*-ZrO_{2-x} was found in 70T30Z and identified by the SADP shown in Fig. 5(c), which was taken along the zone axis of [111]. Based on its structure type, the reflections of the type *odd*, *odd*, *even* were not allowed for *c*-ZrO_{2-x}. This fact was applied to distinguish between *c*-ZrO_{2-x} and *t*-ZrO_{2-x}. However, the {112}-type reflections appeared in the SADPs of *c*-ZrO_{2-x} because a large concentration of oxygen vacancies caused the change in the structure factor of *c*-ZrO_{2-x}. A similar result also indicated the existence of *c*-ZrO_{2-x} from the XRD analyses (Fig. 2).

In sintered 90T10Z, ZrO_2, together with its stabilizer (yttria), was completely dissolved in Ti. Because of the very low solubility of yttrium in Ti (Fig. 4(c)), $Y_2Ti_2O_7$ was precipitated from the α-Ti(Zr, O). Figure 6(a) shows the bright-field image of α-Ti(Zr, O) and $Y_2Ti_2O_7$ in the 90T10Z composite after sintering at 1500°C/1 h. It indicated that both intergranular and intragranular $Y_2Ti_2O_7$ existed in the α-Ti (Zr, O) matrix. The precipitates of $Y_2Ti_2O_7$ were coarsened through the Ostwald ripening effect so that they were spherical in shape. Figures 6(b) and (c) show the SADPs of $Y_2Ti_2O_7$ along the zone axes of [111] and [001], respectively. The calculated lattice parameter of the $Y_2Ti_2O_7$ unit cell was about 11.08 Å. The $Y_2Ti_2O_7$ possesses the pyrochlore structure in which one out of every eight oxygen ions is missing in the stoichiometric fluorite. The ideal $Y_2Ti_2O_7$ structure has a cubic unit cell consisting of eight fluorite-type cells with ordered oxygen vacancies. The calculated lattice parameter of $Y_2Ti_2O_7$ ($a = 11.08$ Å) is approximately twice that of fluorite

Table III. Compositions of ZrO_{2-x} in Various Ti/ZrO_2 Composites After Sintering

Specimens	Composition of ZrO_{2-x} (at.%)†				O/Zr	O/Zr × K-factor‡	ZrO_{2-x} (*x* value)
	Zr	O	Y	Ti			
10T90Z	57.6	40.5	1.8	0.1	0.71	1.39	0.61±0.07
30T70Z	59.4	37.7	1.9	1.1	0.64	1.26	0.74±0.04
50T50Z	61.9	35.7	2.0	0.4	0.58	1.14	0.86±0.05
70T30Z	61.8	33.8	3.8	0.6	0.55	1.08	0.92±0.03

†Used stoichiometric ZrO_2 as a standard. ‡*k*-factor is 1.97.

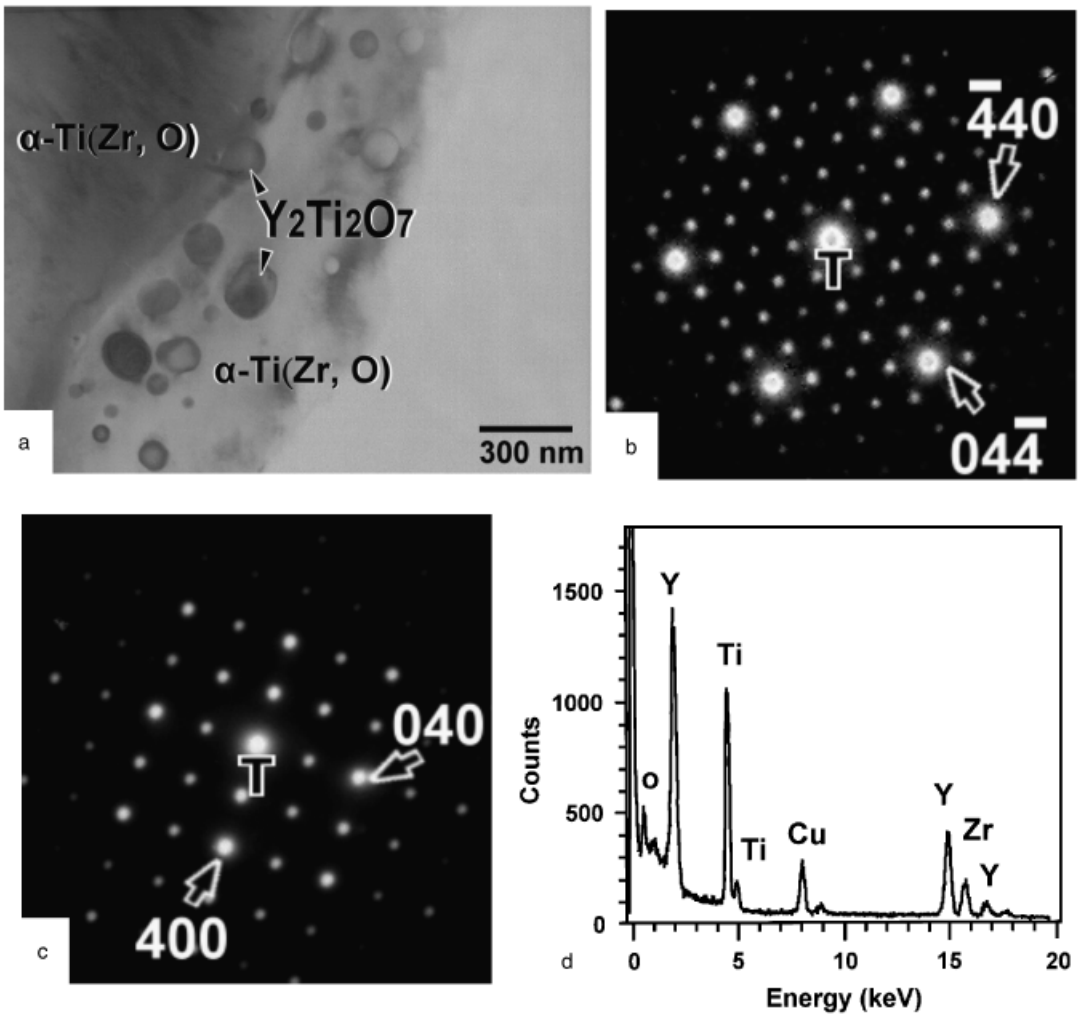

Fig. 6. (a) Transmission electron micrograph (bright-field image) of α-Ti(Zr, O) and $Y_2Ti_2O_7$ in the 90T10Z composite after sintering at 1500°C/1 h; (b) and (c) the selected area diffraction patterns s of the $Y_2Ti_2O_7$ along the zone axes of [111] and [001], respectively; (d) an energy-dispersive spectrum of $Y_2Ti_2O_7$.

($a = 5.10$ Å). The EDS in Fig. 6(d) indicates that $Y_2Ti_2O_7$ contained 26.4 at.% Y, 33.4 at.% Ti, and 40.2 at.% O.

(4) Formation of TiO, Ti_2ZrO, and α-Ti(O, Zr)

Oxygen-deficient ZrO_2 was designated as ZrO_{2-x}, where x is the degree of oxygen deficiency. The value of x increased as the Ti content increased and ranged from 0.61 to 0.92, as listed in Table III. As a reference, stoichiometric ZrO_2 and pure Ti were also annealed under the same sintering conditions. The reference ZrO_2 became oxygen deficient and its composition was measured as ZrO_{2-x} ($x = 0.39$), while the reference Ti dissolved a negligible amount of oxygen ($\approx$0.2 at.%). The concentration of yttria in ZrO_2 increased with the Ti content (Table III). Together with the fact that the Y_2O_3 was nearly insoluble in TiO and α-Ti(Zr, O) (Figs. 3(d) and 4(c)), it was inferred that the stabilizer of ZrO_2 (yttria) was mainly retained in residual ZrO_2 as ZrO_2 particles were gradually dissolved into Ti. Based on XRD and TEM/EDS results, it was the oxygen released from ZrO_2 that resulted in the formation of α-Ti(O), Ti_2ZrO, and/or TiO. If the supply of oxygen from ZrO_2 was sufficient, for example, in the sintered 10T90Z and 30T70Z, TiO was formed. Otherwise, α-Ti(O, Zr) and Ti_2ZrO were formed such as in the specimens containing $<$50 mol% ZrO_2.

Based on commonly cited Ellingham diagrams, Ti should not reduce ZrO_2. Such diagrams have led to erroneous conclusions in some studies.[8,26] Lin *et al.*[8] and Bannister and Barnes[26] hypothesized that Ti was oxidized by residual oxygen in the chamber, resulting in the formation of TiO or TiO_2. TiO could be formed when the vacuum was in the range of 10^{-1}–10^{-2} torr. If the vacuum was poor, TiO_2 was formed and resulted in no stabilization of ZrO_2. While the vacuum level was better than 5×10^{-4} torr, no TiO could be formed and therefore no stabilization of ZrO_2 was observed. In fact, the Ellingham diagram does not accurately describe the reactions in the Ti–ZrO_2 system because it does not account for solution formation or the formation of intermediate compounds like α-Ti(Zr,O), TiO, Ti_2ZrO, and/or ZrO_{2-x}. Based on the present results, it was believed that the reaction between Ti and ZrO_2 was controlled by reduction–dissolution mechanisms. This conclusion was consistent with those observed in the Ti/ZrO_2 diffusion couples, conducted at high temperatures ranging from 1100° to 1550°C by Lin and Lin.[16,17,20,21]

(5) Grain Growth of ZrO_2

The grain size of *m*- or *t*-ZrO_2 in the sintered 10T90Z was about 0.3 μm (Fig. 3(a)) similar to the original ZrO_2 particle size. The formation of TiO effectively retarded the grain growth of ZrO_2 in the sintered 10T90Z. This was consistent with previous results, which indicated that the pinning of the intergranular TiO decreased the grain size of ZrO_2 and improved its strength and thermal shock resistance.[8] However, the grain size of *m*- or *t*-ZrO_2 increased to about 1–2 μm in the sintered 50T50Z (Fig. 4(a)). In the sintered 70T30Z, the *c*-ZrO_2 was found instead of *m*- or *t*-ZrO_2 and its grain size grew to about 2.5–4 μm (Fig. 5(a)). Thus, the ZrO_2 grain size was affected by the Ti content in Ti/ZrO_2 composites. It was believed that oxygen diffu-

Table IV. Reaction Products, Crystal Structures, and Morphology in Ti/ZrO_2 Composites

Specimens	Reaction products	Crystal structures	Morphology
90T10Z	α-Ti(Zr, O)	Hexagonal	Irregular
	Ti_2ZrO	Orthorhombic	Lamellar
	$Y_2Ti_2O_7$	Pyrochlore	Round
70T30Z	α-Ti(Zr, O)	Hexagonal	Irregular
	Ti_2ZrO	Orthorhombic	Lamellar
	c-ZrO_{2-x}	Cubic	Equiaxed
50T50Z	α-Ti(Zr, O)	Hexagonal	Irregular
	Ti_2ZrO	Orthorhombic	Lamellar
	m-ZrO_{2-x}	Monoclinic	Twined
	t-ZrO_{2-x}	Tetragonal	Equiaxed
30T70Z	α-Ti(Zr, O)	Hexagonal	Irregular
	TiO	Cubic (NaCl type)	Irregular
	m-ZrO_{2-x}	Monoclinic	Twined
	t-ZrO_{2-x}	Tetragonal	Equiaxed
10T90Z	TiO	Cubic (NaCl type)	Irregular
	m-ZrO_{2-x}	Monoclinic	Twined
	t-ZrO_{2-x}	Tetragonal	Equiaxed

sion through a vacancy mechanism was predominant for the grain growth of ZrO_2 in the Ti/ZrO_2 composites. Lin and Lin[21] reported that the rate of reduction–dissolution between ZrO_2 and Ti increased with temperature, leading to a significant increase in oxygen vacancies in ZrO_2, which increased diffusion velocities and enhanced the grain growth of ZrO_{2-x}. Previous studies indicated that α-Zr was segregated to the ZrO_2 grain boundaries by the exsolution of zirconium from metastable ZrO_{2-x} in the region far away from the original interface during cooling.[17,21] However, no intergranular α-Zr was found in Ti/ZrO_2 composites as zirconium was readily dissolved in the abutting Ti to form α-Ti(Zr, O) in this study.

According to the foregoing discussion, the reaction products, crystal structures, and morphology in Ti/ZrO_2 composites sintered at 1500°C/1 h are summarized in Table IV. The interfacial reactions between Ti and ZrO_2 powders are briefly described as follows: During sintering, Zr and O diffused into Ti, whereas Ti simultaneously diffused into ZrO_2. The TiO was formed in the sintered 10T90Z and 30T70Z, because a sufficient amount of oxygen, released from ZrO_2, was dissolved in the Ti. For the sintered 50T50Z, 70T30Z, and 90T10Z, α-Ti(Zr, O) and Ti_2ZrO were formed because smaller amounts of oxygen were supplied by ZrO_2. Both *t*- and *m*-ZrO_{2-x} were found in the sintered 10T90Z, 30T70Z, and 50T50Z, while *c*-ZrO_{2-x} was stabilized by a high concentration of the retained yttria and oxygen vacancies in the sintered 70T30Z. In the sintered 90T10Z, ZrO_2 particles were almost dissolved in α-Ti(Zr, O), which resulted in the precipitation of $Y_2Ti_2O_7$.

IV. Conclusions

(1) Powder mixtures of Ti and 3 mol% Y_2O_3-PSZ in various ratios were sintered at 1500°C for 1 h in an argon atmosphere. The microstructures and reaction products of the Ti/ZrO_2 composites depended on the Ti/ZrO_2 ratio.

(2) Ti reacted with and was mutually soluble in ZrO_2, resulting in the formation of α-Ti(O, Zr), Ti_2ZrO, and/or TiO. Oxygen atoms, contained in α-Ti(O, Zr), Ti_2ZrO, and/or TiO, were extracted from ZrO_2, whereby oxygen-deficient ZrO_2 was produced.

(3) In the specimens with $\leq$30 mol% Ti, the relatively small Ti/ZrO_2 ratio led to the formation of TiO as oxygen could be sufficiently supplied by excess ZrO_2.

(4) Relatively large Ti/ZrO_2 ratios resulted in the formation of α-Ti(Zr, O) as well as Ti_2ZrO in the specimens with $\geq$ 50 mol% Ti, with no TiO being found.

(5) Both *m*-ZrO_{2-x} and *t*-ZrO_{2-x} were found in specimens with $\leq$50 mol% Ti; however, *c*-ZrO_{2-x} was formed in the specimens with 70 mol% Ti as it contained a high concentration of retained yttria and oxygen vacancies in ZrO_2.

(6) In the specimen with 90 mol% Ti, ZrO_2 particles were almost dissolved in Ti, being accompanied of simultaneous precipitation of $Y_2Ti_2O_7$.

Acknowledgments

The authors would like to express their sincere gratitude to Mr. Ming-Chung Li and Wei-Chen Wang for preparing the Ti/ZrO_2 composite specimens.

References

[1]R. C. Garvie, R. H. J. Hannink, and R. T. Pascoe, "Ceramic Steel," *Nature (London)*, **258**, 703–4 (1975).
[2]R. H. J. Hannink, P. M. Kelly, and B. C. Muddle, "Transformation Toughening in Zirconia-Containing Ceramics," *J. Am. Ceram. Soc.*, **83** [3] 461–87 (2000).
[3]B. C. Weber, H. J. Garrett, F. A. Mauer, and M. A. Schwartz, "Observations on the Stabilization of Zirconia," *J. Am. Ceram. Soc.*, **39** [6] 197–207 (1956).
[4]R. Ruh, "Reaction of Zirconia and Titanium at Elevated Temperatures," *J. Am. Ceram. Soc.*, **46** [7] 301–6 (1963).
[5]R. Ruh, N. M. Tallan, and H. A. Lipsitt, "Effect of Metal Additions on the Microstructure of Zirconia," *J. Am. Ceram. Soc.*, **47** [12] 632–5 (1964).
[6]A. Arias, "Thermal Shock Resistance of Zirconia With 15 mol% Titanium," *J. Am. Ceram. Soc.*, **49** [6] 334–8 (1966).
[7]A. Arias, "Mechanism by Which Metal Additions Improve the Thermal Shock Resistance of Zirconia," *J. Am. Ceram. Soc.*, **49** [6] 339–41 (1966).
[8]C. L. Lin, D. Gan, and P. Shen, "Stabilization of Zirconia Sintered With Titanium," *J. Am. Ceram. Soc.*, **71** [8] 624–9 (1988).
[9]L. D. Teng, F. M. Wang, and W. C. Li, "Thermodynamics and Microstructure of Ti–ZrO_2 Metal–Ceramic Functionally Graded Materials," *Mater. Sci. Eng. A*, **293**, 130–6 (2000).
[10]L. D. Teng, W. C. Li, and F. M. Wang, "Effect of Ti Content on the Martensitic Transformation in Zirconia for Ti-ZrO_2 Composites," *J. Alloys Compds.*, **319**, 228–32 (2001).
[11]G. Economos and W. D. Kingery, "Metal–Ceramic Interactions: II, Metal Oxide Interfacial Reactions at Elevated Temperatures," *J. Am. Ceram. Soc.*, **36** [12] 403–9 (1953).
[12]B. C. Weber, W. M. Thompson, H. O. Bielstein, and M. A. Schwartz, "Ceramic Crucible for Melting Titanium," *J. Am. Ceram. Soc.*, **40** [11] 363–73 (1957).
[13]R. F. Domagala, S. R. Lyon, and R. Ruh, "The Pseudobinary Ti–ZrO_2," *J. Am. Ceram. Soc.*, **56** [11] 584–7 (1973).
[14]K. F. Lin and C. C. Lin, "Transmission Electron Microscope Investigation of the Interface Between Titanium and Zirconia," *J. Am. Ceram. Soc.*, **82** [11] 3179–85 (1999).
[15]J. Zhu, A. Kamiya, T. Yamada, W. Shi, K. Naganuma, and K. Mukai, "Surface Tension, Wettability and Reactivity of Molten Titanium in Ti/Yttria-Stabilized Zirconia System," *Mater. Sci. Eng. A*, **A327**, 117–27 (2002).
[16]K. L. Lin and C. C. Lin, "Microstructural Evolution and Formation Mechanism of the Interface Between Zirconia and Titanium Annealed at 1550°C," *J. Am. Ceram. Soc.*, **89** [4] 1400–8 (2005).
[17]K. L. Lin and C. C. Lin, "Temperature Dependence of the Interfacial Reaction Between Titanium and Zirconia Annealed Between 1100° and 1550°C," *J. Am. Ceram. Soc.*, **90** [3] 893–9 (2007).
[18]K. F. Lin and C. C. Lin, "Interfacial Reactions Between Zirconia and Titanium," *Scripta Metall.*, **39** [10] 1333–8 (1998).
[19]K. F. Lin and C. C. Lin, "Interfacial Reactions Between Ti–6Al–4V Alloy and Zirconia Mold During Casting," *J. Mater. Sci.*, **34**, 5899–906 (1999).
[20]K. L. Lin and C. C. Lin, "Ti_2ZrO Phases Formed in the Titanium and Zirconia Interface After Reaction at 1550°C," *J. Am. Ceram. Soc.*, **88** [5] 1268–72 (2005).
[21]K. L. Lin and C. C. Lin, "Zirconia-Related Phases in the Zirconia/Titanium Diffusion Couple After Annealing at 1100° to 1550°C," *J. Am. Ceram. Soc.*, **88** [10] 2928–34 (2005).
[22]G. Cliff and G. W. Lorimer, "The Quantitative Analysis of Thin Specimens," *J. Microsc.*, **130** [3] 203–7 (1975).
[23]M. Rühle, N. Claussen, and A. H. Heuer, "Microstructural Studies of Y_2O_3-Containing Tetragonal ZrO_2 Polycrystals (Y-TZP)"; pp. 352–70 in *Advances in Ceramics, Vol. 12, Science and Technology of Zirconia II*, Edited by N. Claussen, M. Rühle, and A. H. Heuer. American Ceramic Society, Columbus, OH, 1984.
[24]A. H. Heuer and M. Rühle, "On the Nucleation of the Martensitic Transformation in Zirconia (ZrO_2)," *Acta. Metall.*, **33** [12] 2101–12 (1985).
[25]P. C. Wahlbeck and P. W. Gilles, "Reinvestigation of the Phase Diagram for the System Titanium–Oxygen," *J. Am. Ceram. Soc.*, **49** [4] 180–3 (1966).
[26]M. J. Bannister and J. M. Barnes, "Solubility of TiO_2 in ZrO_2," *J. Am. Ceram. Soc.*, **69** [11] C-269–71 (1986). □